Contrib Mineral Petrol (2007) 154:479–490
DOI 10.1007/s00410-007-0206-8

ORIGINAL PAPER

Magnetite scavenging and the buoyancy of bubbles in magmas. Part 2: Energetics of crystal-bubble attachment in magmas

Guilherme A. R. Gualda · Mark S. Ghiorso

Received: 18 October 2005 / Accepted: 29 March 2007 / Published online: 26 June 2007

Abstract The fate of pre-eruptive bubbles depends largely on their buoyancy, which can be strongly modified by the presence of crystals attached to the bubble–melt interface. We define the attachment energy and attachment force as those resulting from the attachment of a crystal to a bubble. The attachment energy is such that (1) attachment of crystals to bubbles is always favored energetically, and (2) oxide minerals attach to bubbles much more strongly than silicates, because the attachment energy is a strong function of the wetting angle. Attaching crystals to bubbles can cause bubble–crystal pairs to become neutrally buoyant. There is a critical bubble radius below which the attachment force will be strong enough to keep the pair together; we show that crystals as large as 1 mm in diameter can form neutrally buoyant pairs. For early erupted Bishop magma, if all magnetite forms neutrally buoyant pairs with gas bubbles, ca. 0.1–0.2 vol% gas can be stored in the magma; 2–3 vol% of gas can be accounted for if all minerals form neutrally buoyant aggregates. These values are an order of magnitude lower than what is inferred from melt inclusions. Hence, both magnetite-free and magnetite-rich bubbles might have existed, but only a very small fraction of them could have been neutrally buoyant. Importantly, an intrinsic association between magnetite crystals and bubbles is expected. However, most magnetite crystals in the early erupted Bishop are free of bubbles; the puzzling conclusion is that nucleation away from crystals is favored over heterogeneous nucleation on crystal substrates.

Electronic Supplementary Material The online version of this article (doi:10.1007/s00410-007-0206-8) contains supplementary material, which is available to authorized users.

Communicated by T.L. Grove.

G. A. R. Gualda (✉)
Department of the Geophysical Sciences,
The University of Chicago, 5734 S. Ellis Ave.,
Chicago, IL 60637, USA
e-mail: ggualda@uchicago.edu

M. S. Ghiorso
OFM Research, West, 7336 24th Ave. NE,
Seattle, WA 98115, USA

Introduction

The propellant for explosive volcanic eruptions is the exsolution and growth of bubbles in ascending magmas (Wilson et al. 1980). It is generally assumed that when eruptions are triggered, magmas are bubble-free, and all the vesicularity observed in pumice is due to nucleation and growth during ascent. This assumption may seem reasonable at first given that: (1) nucleation may be limited under pre-eruptive magmatic conditions due to the relatively high supersaturation implicated by experiments (Mangan and Sisson 2000); (2) even if bubbles form in the pre-eruptive magma, they tend to rise and escape from the magma body.

Decompression experiments show that bubbles tend to nucleate on magnetite crystals (Hurwitz and Navon 1994; Mangan and Sisson 2000, 2005), what greatly reduces the supersaturation needed for nucleation. In the case of the Bishop Tuff, it has been argued that an exsolved gas phase must have been present in order to account for the evolution of H_2O/CO_2 ratios with melt differentiation (Wallace et al. 1995, 1999). Furthermore, in the accompanying paper (Gualda and Anderson 2007), we present direct evidence for the presence of pre-eruptive bubbles in the Bishop magma, in the form of a large vesicle with abun-

dant magnetite crystals attached to its walls. Hence, we conclude that bubbles do nucleate under pre-eruptive conditions.

The fate of pre-eruptive bubbles depends directly on their buoyancy, but the buoyancy of bubbles in magma can be strongly modified by the presence of crystals attached to the bubble–melt interface. That such attachment occurs is indicated by experiments (Hurwitz and Navon 1994; Mangan and Sisson 2000, 2005) and observations (Gualda and Anderson 2007), and can be readily explained theoretically. Whether, however, magnetite crystals and bubbles can be held together by interface forces is yet uncertain. In this contribution, we use the available knowledge on surface energies of phases under magmatic conditions to explore this problem.

Furthermore, while experiments and observations indicate an intrinsic association between magnetite and bubbles, no such association between bubbles and quartz or feldspars is implicated (Mangan and Sisson 2000). We show that this distinction is to be expected, based on available experimental data on the wetting angles of silicate and oxide phases in silicate melts.

The formation of bubble-magnetite aggregates has important petrologic consequences. Particularly, it can be argued that if bubbles collect magnetite crystals efficiently, they may become neutrally buoyant, giving rise to a permanent exsolved-gas reservoir in magmas. We test this idea using the available data for the Bishop Tuff.

Theory

The attachment energy

Definitions

The change in free energy due to the attachment of a bubble to a mineral substrate is simply the change in surface energy between the state where bubble and mineral are apart (Fig. 1a) and that where bubble and mineral are attached (Fig. 1b). We call this energy change the attachment energy ($\Delta\sigma$):

$$\Delta\sigma = \sigma^{\text{Joint}} - \sigma^{\text{Separate}} \tag{1}$$

where the components σ^{Separate} and σ^{Joint} are given by:

$$\begin{aligned}\sigma^{\text{Separate}} &= A^{\text{Separate}}_{\text{Bubble-Liquid}}\,\sigma_{\text{Bubble-Liquid}} \\ &\quad + A^{\text{Separate}}_{\text{Mineral-Liquid}}\,\sigma_{\text{Mineral-Liquid}}\end{aligned} \tag{2}$$

$$\begin{aligned}\sigma^{\text{Joint}} &= A^{\text{Joint}}_{\text{Bubble-Liquid}}\,\sigma_{\text{Bubble-Liquid}} \\ &\quad + A^{\text{Joint}}_{\text{Mineral-Liquid}}\,\sigma_{\text{Mineral-Liquid}} \\ &\quad + A^{\text{Joint}}_{\text{Bubble-Mineral}}\,\sigma_{\text{Bubble-Mineral}}\end{aligned} \tag{3}$$

where A denotes area, and σ denotes surface energy (per unit area).

The attachment energy, after simplifications, becomes:

$$\begin{aligned}\Delta\sigma &= \left(A^{\text{Joint}}_{\text{Bubble-Liquid}} - A^{\text{Separate}}_{\text{Bubble-Liquid}}\right)\sigma_{\text{Bubble-Liquid}} \\ &\quad + A^{\text{Joint}}_{\text{Bubble-Mineral}}\,\sigma_{\text{Bubble-Mineral}} \\ &\quad - A^{\text{Joint}}_{\text{Bubble-Mineral}}\,\sigma_{\text{Mineral-Liquid}}\end{aligned} \tag{4}$$

The attachment energy ($\Delta\sigma$) is the total change in free energy from the fully separated state to the fully attached state. However, the energy that binds bubble and mineral together after attachment is given by what we may call the adhesion energy ($\Delta\sigma^{\text{Adhesion}}$):

$$\begin{aligned}\Delta\sigma^{\text{Adhesion}} &= A^{\text{Joint}}_{\text{Bubble-Mineral}} \\ &\quad \left(\sigma_{\text{Bubble-Mineral}} - \sigma_{\text{Bubble-Liquid}} - \sigma_{\text{Mineral-Liquid}}\right)\end{aligned} \tag{5}$$

The remainder of the energy change encompassed by $\Delta\sigma$ corresponds to the energy necessary to deform the bubble

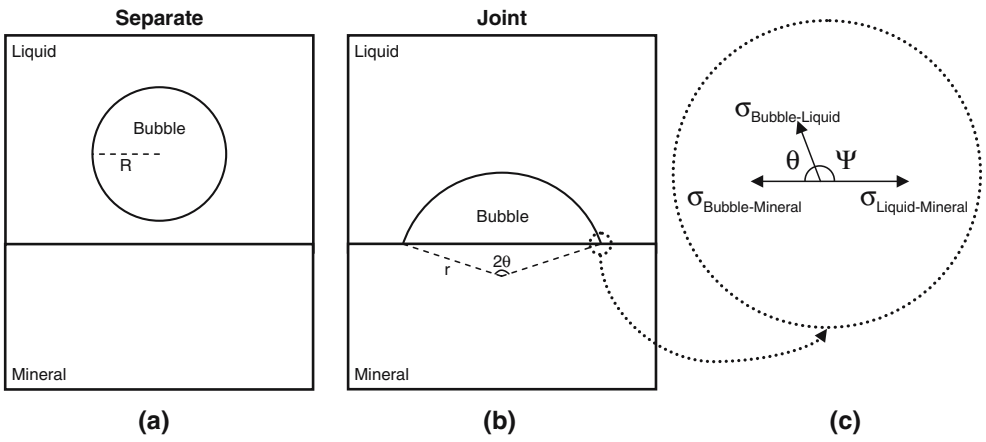

Fig. 1 Diagrams illustrating two possible configurations for coexisting bubble, liquid and mineral. In **a** the bubble is entirely within the liquid, while in **b** the bubble is attached to the solid substrate. The balance of forces at the bubble–mineral contact point is shown in **c**. In the text, geometries are considered to be three-dimensional, and can be derived from the geometries shown by assuming cylindrical symmetry for the bubble

from the separated configuration to the joint configuration, and it would be appropriate to call this the deformation energy ($\Delta\sigma^{\text{Deformation}}$):

$$\Delta\sigma^{\text{Deformation}} = \left(A^{\text{Joint}}_{\text{Bubble}-\text{Liquid}} + A^{\text{Joint}}_{\text{Bubble}-\text{Mineral}} - A^{\text{Separate}}_{\text{Bubble}-\text{Liquid}}\right)\sigma_{\text{Bubble}-\text{Liquid}} \quad (6)$$

The total energy change can then be understood as the combination of a deformation step given by Eq. 6, and an adhesion step described by Eq. 5 (Adamson and Gast 1997):

$$\Delta\sigma = \Delta\sigma^{\text{Deformation}} + \Delta\sigma^{\text{Adhesion}} \quad (7)$$

The significance of these two components will be discussed in a later section.

Relation to wetting angle

In this contribution, we aim at solving Eqs. 4–6 as a function of the wetting angle. The surface energies in Eqs. 4–6 can be related to each other by using the definition of the wetting angle (Ψ; see, for instance, Adamson and Gast 1997):

$$\cos\Psi = \frac{\sigma_{\text{Bubble}-\text{Mineral}} - \sigma_{\text{Mineral}-\text{Liquid}}}{\sigma_{\text{Bubble}-\text{Liquid}}} \quad (8)$$

The wetting angle Ψ is analogous to θ in Fig. 1, except that Ψ is the angle formed when a liquid wets the surface of the mineral. The angle θ is simply related to the wetting angle Ψ ($\theta = 180 - \Psi$), such that:

$$\sigma_{\text{Bubble}-\text{Liquid}}\cos\theta = \sigma_{\text{Mineral}-\text{Liquid}} - \sigma_{\text{Bubble}-\text{Mineral}} \quad (9)$$

Equations 4 and 5 then reduce to:

$$\Delta\sigma = \left(A^{\text{Joint}}_{\text{Bubble}-\text{Liquid}} - A^{\text{Separate}}_{\text{Bubble}-\text{Liquid}} - A^{\text{Joint}}_{\text{Bubble}-\text{Mineral}}\cos\theta\right)\sigma_{\text{Bubble}-\text{Liquid}} \quad (10)$$

$$\Delta\sigma^{\text{Adhesion}} = -A^{\text{Joint}}_{\text{Bubble}-\text{Mineral}}(1+\cos\theta)\,\sigma_{\text{Bubble}-\text{Liquid}} \quad (11)$$

It is relevant to note here that the only surface energy term in Eqs. 6, 10, and 11 is $\sigma_{\text{Bubble–Liquid}}$.

To isolate the effect of the wetting angle, the areas in Eqs. 4–6 can be described as a function of θ and the original bubble volume. We assume that the detached bubble is spherical, and the attached bubble is a spherical cap (Weisstein 2007). The implicit assumption is that gravitational forces are negligible; the appropriateness of this assumption will be discussed in a later section.

From Fig. 1, it can be deduced that:

$$A^{\text{Separate}}_{\text{Bubble}-\text{Liquid}} = 4\pi R^2 \quad (12a)$$

$$A^{\text{Joint}}_{\text{Bubble}-\text{Liquid}} = 2\pi r^2(1-\cos\theta) \quad (12b)$$

$$A^{\text{Joint}}_{\text{Bubble}-\text{Mineral}} = \pi(r\sin\theta)^2 \quad (12c)$$

The volume of the spherical cap occupied by the bubble in Fig. 1b can be computed as:

$$V_{\text{Bubble}} = \frac{1}{3}\pi r^3\left[2-3\cos(\theta)+\cos^3(\theta)\right] \quad (13)$$

As the volume of the detached spherical bubble (Fig. 1a) is the same as the volume of the attached bubble (Fig. 1b), it follows from Eq. 13 that:

$$r = R\left[\frac{4}{2-3\cos(\theta)+\cos^3(\theta)}\right]^{1/3} \quad (14)$$

Substituting Eqs. 12a and 14 into 6, 10, and 11 leads to:

$$\Delta\sigma = 4\pi R^2\left[\left(\frac{2-3\cos(\theta)+\cos^3(\theta)}{4}\right)^{1/3} - 1\right]\sigma_{\text{Bubble}-\text{Liquid}} \quad (15)$$

$$\Delta\sigma^{\text{Adhesion}} = -\pi R^2\left[\sin^2\theta\,(\cos\theta+1)\left(\frac{4}{2-3\cos(\theta)+\cos^3(\theta)}\right)^{2/3}\right]\sigma_{\text{Bubble}-\text{Liquid}} \quad (16)$$

$$\Delta\sigma^{\text{Deformation}} = \pi R^2\left[(2-2\cos\theta+\sin^2\theta)\left(\frac{4}{2-3\cos(\theta)+\cos^3(\theta)}\right)^{2/3} - 4\right]\sigma_{\text{Bubble}-\text{Liquid}} \quad (17)$$

The significance of these expressions is hard to grasp due to their complexity. Equation 15 can be much simplified by using Eq. 13:

$$\Delta\sigma = 3V_{\text{Bubble}}\left[\frac{1}{r}-\frac{1}{R}\right]\sigma_{\text{Bubble}-\text{Liquid}} \quad (18)$$

Because $R \leq r$, then it follows that $\Delta\sigma \leq 0$. In other words, the attachment of a bubble to a mineral substrate is always favored energetically, such that the configuration shown in Fig. 1b is always the thermodynamically stable

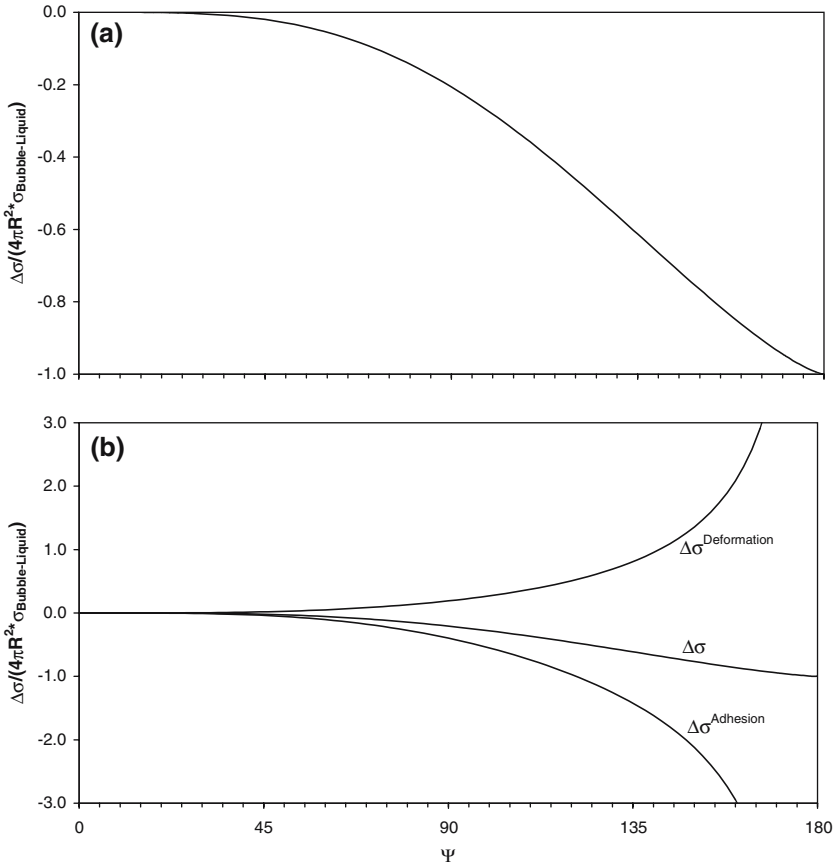

Fig. 2 **a** Variation in the attachment energy (normalized to the area of the detached bubble and the bubble–liquid surface energy) as a function of the wetting angle Ψ. Note that $\Delta\sigma$ is always negative, but its absolute value is rather small for $\Psi < 25$ and increases significantly for $\Psi > 45$. **b** Contributions of $\Delta\sigma^{Adhesion}$ and $\Delta\sigma^{Deformation}$ to $\Delta\sigma$, all normalized like in **a**. Both $\Delta\sigma^{Adhesion}$ and $\Delta\sigma^{Deformation}$ are very small for $\Psi < 25$ and increase very rapidly for large Ψ. $\Delta\sigma^{Deformation}$ and $\Delta\sigma^{Adhesion}$ are the barriers to attachment and detachment, respectively, such that with increasing Ψ, the attachment efficiency decreases, but once bubble and crystal are attached, it becomes increasingly more difficult to detach, and the overall energy reduction increases (see text for details)

configuration, regardless of the wetting angle. This has important consequences to the fate of bubbles in magmas, because a bubble plus crystal aggregate will be less buoyant than a solitary bubble (see Sect. 3).

The variation of $\Delta\sigma$ as a function of the wetting angle is shown in Fig. 2a, while the relative contributions of $\Delta\sigma^{Adhesion}$ and $\Delta\sigma^{Deformation}$ to $\Delta\sigma$ are plotted in Fig. 2b. What Fig. 2a shows is that, even though always negative, $\Delta\sigma$ is very small for $\Psi < 25$, but starts increasing much more rapidly with increasing wetting angle. Hence, the larger the wetting angle, the stronger the attachment of bubble and mineral.

Figure 2b shows that both contributions to $\Delta\sigma$ are small for $\Psi < 25$, and increase markedly with wetting angle. It can also be seen that $\Delta\sigma^{Deformation}$ is always positive, as it corresponds to the energy spent deforming the bubble from the spherical shape in Fig. 1a to the spherical cap shape in Fig. 1b (Adamson and Gast 1997). In this sense, it can be taken to represent a barrier to attachment. The inference is then that the barrier is small for small Ψ, but increases significantly with increasing Ψ, such that the attachment efficiency tends to decrease with increasing wetting angle. The contribution of $\Delta\sigma^{Adhesion}$ arises from the conversion of Bubble–Liquid and Liquid–Mineral interfaces into a single Bubble–Mineral interface. This contribution is always negative, and becomes more negative with increasing wetting angle; in fact, Fig. 2b shows that the absolute value of $\Delta\sigma^{Adhesion}$ increases faster than that of $\Delta\sigma^{Deformation}$. While $\Delta\sigma^{Deformation}$ can be understood as a barrier to attachment, $\Delta\sigma^{Adhesion}$ can be interpreted to be the equivalent barrier to detachment. The inference is thus that the higher the wetting angle, the harder it is to detach bubble from mineral.

The interplay between $\Delta\sigma^{Adhesion}$ and $\Delta\sigma^{Deformation}$ is an interesting one with significant petrologic implications. For a given system, for a mineral with small wetting angle (i.e. $\Psi < 25$), the barriers to attachment or detachment are small, as also is the net energy reduction due to attachment. It is to be expected that, in a dynamic system, even if mineral and bubble do attach, they can be easily detached, and bubble–mineral aggregates are not particularly stable. On the other hand, for a mineral with large wetting angle (e.g. $\Psi > 45$), the efficiency of bubble–mineral attachment tends to be diminished. However, once attached, the total energy difference is large, and the barrier to detachment even larger, such that bubble–mineral aggregates are bound to be preserved. This result is at the heart of the experimental and petrographic observations of a preferred

magnetite-bubble association (in relation to felsic silicates) in rhyolitic systems (Gualda and Anderson 2007; Hurwitz and Navon 1994; Mangan and Sisson 2000, 2005).

Relative attachment energy

One of our goals here is to compare the attachment properties of different minerals and bubbles in magmatic conditions. Such a comparison can be made in a quantitative way by using the ratios between Eqs. 15, 16, and 17 for different wetting angles:

$$\frac{\Delta\sigma_{\text{Mineral1}}}{\Delta\sigma_{\text{Mineral2}}}=\frac{\left(2-3\cos(\theta_{\text{Mineral1}})+\cos^3(\theta_{\text{Mineral1}})\right)^{1/3}-4^{1/3}}{\left(2-3\cos(\theta_{\text{Mineral2}})+\cos^3(\theta_{\text{Mineral2}})\right)^{1/3}-4^{1/3}} \tag{19}$$

$$\frac{\Delta\sigma^{\text{Adhesion}}_{\text{Mineral1}}}{\Delta\sigma^{\text{Adhesion}}_{\text{Mineral2}}}=\frac{\frac{\sin^2\theta_{\text{Mineral1}}(\cos\theta_{\text{Mineral1}}+1)}{\left(2-3\cos(\theta_{\text{Mineral1}})+\cos^3(\theta_{\text{Mineral1}})\right)^{2/3}}}{\frac{\sin^2\theta_{\text{Mineral2}}(\cos\theta_{\text{Mineral2}}+1)}{\left(2-3\cos(\theta_{\text{Mineral2}})+\cos^3(\theta_{\text{Mineral2}})\right)^{2/3}}} \tag{20}$$

$$\frac{\Delta\sigma^{\text{Deformation}}_{\text{Mineral1}}}{\Delta\sigma^{\text{Deformation}}_{\text{Mineral2}}}=\frac{\frac{\left(2-2\cos\theta_{\text{Mineral1}}+\sin^2\theta_{\text{Mineral1}}\right)}{\left(2-3\cos(\theta_{\text{Mineral1}})+\cos^3(\theta_{\text{Mineral1}})\right)^{2/3}}-4^{1/3}}{\frac{\left(2-2\cos\theta_{\text{Mineral2}}+\sin^2\theta_{\text{Mineral2}}\right)}{\left(2-3\cos(\theta_{\text{Mineral2}})+\cos^3(\theta_{\text{Mineral2}})\right)^{2/3}}-4^{1/3}} \tag{21}$$

In Fig. 3, we show the variation in the ratios Eqs. 19–21 as a function of $\Psi_{\text{Mineral 1}}$ for several values of $\Psi_{\text{Mineral 2}}$. It can be seen that, especially for low values of $\Psi_{\text{Mineral 2}}$, all 3 ratios increase very rapidly with increasing $\Psi_{\text{Mineral 1}}$. As we will see below, this is particularly interesting in cases where minerals of varied wetting angle are present in the same system.

Application to natural magmas

In order to consider relevant magmatic situations, knowledge of the wetting angles for different minerals under the same conditions is necessary. The advantage of Eqs. 19–21 is that no knowledge of $\sigma_{\text{Bubble–Liquid}}$ is necessary, as long as the comparison is between minerals in the same magma.

Relatively little data are available on the wetting angles of different minerals in the same liquid and at the same conditions. For silicic magmas in particular, some information is available from experiments (Hurwitz and Navon 1994; Laporte 1994; Mangan and Sisson 2005; Mangan, et al. 2004), which indicate relatively low wetting angles for felsic silicates (i.e. quartz and feldspar, Ψ < 20–25), with significantly higher values for magnetite (i.e. Ψ = 35°–50°). In the companion paper (Gualda and Anderson 2007), we have shown that magnetite wetting angles can be determined in a natural sample from the Bishop Tuff, and yield values in the range 45°–50°, in agreement with the experimental data of Mangan and Sisson (2005).

We can now solve Eqs. 19–21 and compare the attachment energies of magnetite ($\Psi_{\text{Magnetite}} \approx$ 45°–50°), and that for felsic silicates ($\Psi_{\text{Silicates}} \approx$ 5°–25°), which results:

$$9<\frac{\Delta\sigma_{\text{Magnetite}}}{\Delta\sigma_{\text{Silicates}}}<8,000 \tag{22}$$

A notable dataset exists for wetting angles of several minerals in mafic magma (Schafer and Foley 2002), which includes wetting angles for several crystal faces of spinel, diopside, enstatite, and forsterite in a basaltic melt. Their data show that spinel has wetting angles between 35° and 42°, while the various mafic silicates are in the range 2°–24°, which leads to:

$$4<\frac{\Delta\sigma_{\text{Spinel}}}{\Delta\sigma_{\text{Silicates}}}<1.6\cdot10^5 \tag{23}$$

It should be noted that diopside and forsterite are very anisotropic, with wetting angles close to the minimum of 2° on (010) faces and maximum of 24° on (100) faces, while enstatite is more isotropic, with corresponding wetting angles of 6° and 15°. As expected, spinel is much less anisotropic, with most wetting angles close to 35° (Schafer and Foley 2002). Consequently, values for the ratio $\Delta\sigma_{\text{Spinel}}/\Delta\sigma_{\text{Silicates}}$ are more likely close to 50–300.

In any case, it becomes clear that the energy reduction due to attachment of spinel to a bubble is much larger than the energy reduction resulting from the attachment of a mafic silicate to the same bubble in this basaltic liquid. Hence, we expect that spinel grains will attach to the bubble much more strongly than any of the mafic silicates. The case is very similar to that of magnetite and felsic silicates in rhyolites.

The similar results in both systems should not be surprising. Interface energies result from the mismatch in structure and differences in the bonding between the two phases separated by that interface. Under this perspective, it is easy to explain the large wetting angles for spinel and magnetite and the relatively low wetting angles for the mafic and felsic silicates in basalts and rhyolites, respectively. Spinel and magnetite have structures and bonding much different from that of basaltic or rhyolitic liquids, which, in turn, are more similar to that of mafic and felsic silicate minerals (Mysen and Richet 2005). Hence, we predict that any oxide mineral in a silicate liquid will have wetting angles much larger than any silicate mineral.

The important conclusion from this section is that, in silicate melts, the reduction in surface energy resulting from attachment of an oxide to a bubble is at least one order of magnitude larger (and potentially much larger)

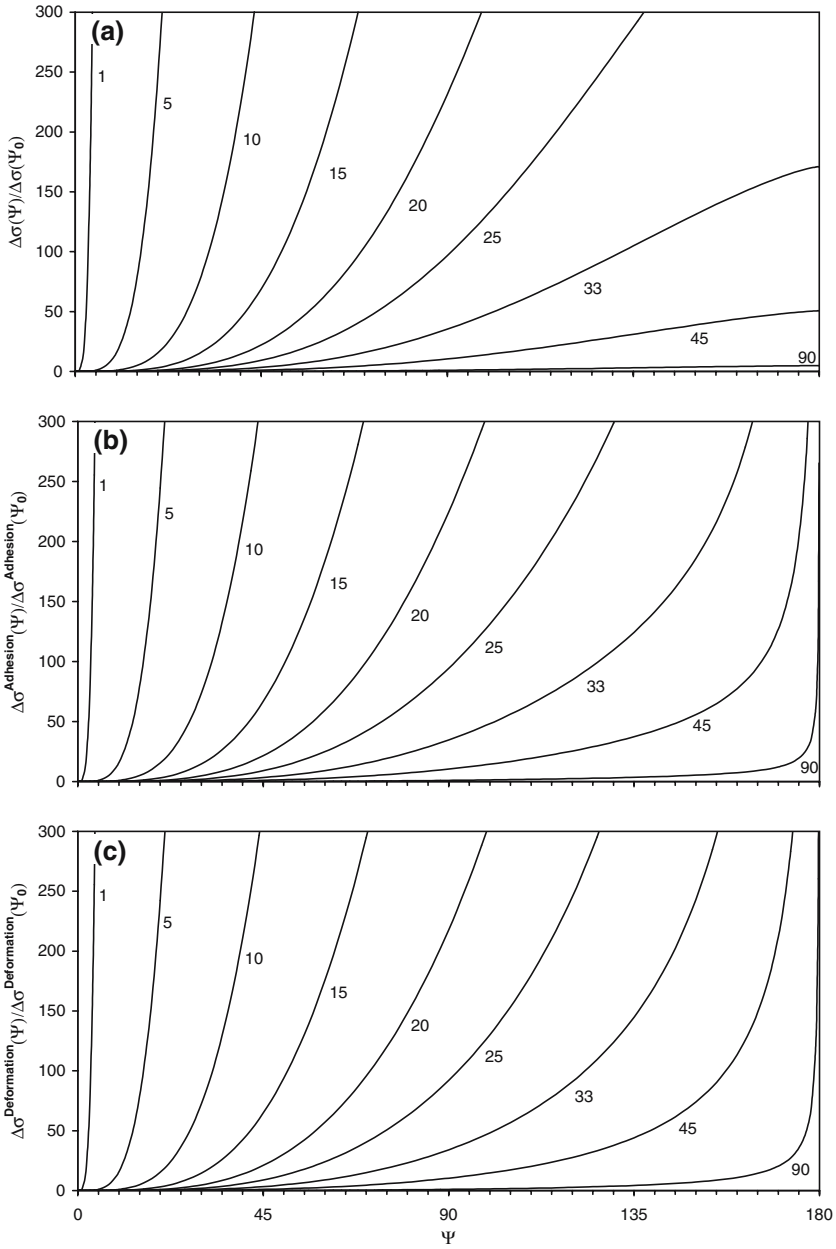

Fig. 3 **a** Variation in the ratio between attachment energy for two solids with wetting angles Ψ and Ψ_0 as a function of the wetting angle Ψ. Different curves correspond to distinct values of Ψ_0, as indicated. Curves for values of Ψ_0 smaller than 15° are very steep and lead to very high $\Delta\sigma_{\text{Mineral 1}}/\Delta\sigma_{\text{Mineral 2}}$ ratios even for relatively low wetting angles (i.e. $\Psi < 45°$). (b) and (c) are the analogous plots for $\Delta\sigma^{Adhesion}$ and $\Delta\sigma^{Deformation}$, respectively. Notice the similarity of the three plots for $\Psi_0 \leq 15$

than the surface energy reduction due to attachment of a silicate mineral to a bubble.

Given the similarity between the shapes of Eqs. 19, 20, and 21, it can also be concluded that the attachment and detachment barriers will be significantly larger for oxides than for silicates, as discussed above (cf. Fig. 3).

The attachment force

In the preceding section we showed that there is always a surface energy reduction upon attachment of a crystal to a bubble, irrespective of the size of the bubble. In magmatic conditions, however, a crystal–bubble aggregate will only be stable if the attachment force is stronger than the gravitational force that tends to separate the two particles.

Derivation

In order to convert from the attachment energy to an attachment force, the equilibrium configuration presented in Fig. 1c must be considered. Equation 9 is a definition of the wetting angle based on the balance of forces in the horizontal direction. The force that keeps the particles together ($F^{\text{Attachment}}$) corresponds to the vertical component of the same balance of forces. For the spherical cap considered here, this force corresponds to:

$$F^{\text{Attachment}} = \oint (\vec{\sigma} \bullet \hat{z})\, \mathrm{d}s = 2\pi\,(r \sin\theta)\,(\sigma_{\text{Bubble-Liquid}} \sin\theta)$$
$$F^{\text{Attachment}} = 2\pi R\ \sin^2\theta \left[\frac{4}{2 - 3\cos(\theta) + \cos^3(\theta)}\right]^{1/3} \sigma_{\text{Bubble-Liquid}} \quad (24)$$

where $(\vec{\sigma} \bullet \hat{z})$ is the vertical component (i.e. orthogonal to the surface of the solid phase in Fig. 1b) of the resultant shown in Fig. 1c, which is integrated over the perimeter of the surface cap.

The variation of the attachment force with wetting angle is illustrated in Fig. 4. The attachment force is a strong function of Ψ. Interestingly, the curve goes through a maximum at Ψ= 114.5°, rather than at 90° as would be expected from inspection of Fig. 1c. The reason for this is that the attachment force depends not only on the vertical component of $\sigma_{\text{Bubble–Liquid}}$, but also on the radius of the contact surface, both of which are functions of the wetting angle.

Similarly to the approach used for the attachment energy (see Sect. 2.1.3), relative attachment forces can be calculated. As observed in Fig. 5, the variation in relative attachment force is large when one of the mineral phases involved has low wetting angle (i.e. <15°), while the variation is limited otherwise. In the cases considered above, the ratio between the attachment force for magnetite and the attachment force for felsic silicates in silicic melt is close to 5, and the situation is similar for spinel and mafic silicates in basaltic melts.

Neutral buoyancy of crystal–bubble pairs

One interesting consequence of the attachment of grains to a bubble is that this can be a mechanism which causes these bubble–crystal pairs to be neutrally buoyant, preventing bubbles from rising and crystals from sinking relative to the melt.

The buoyancy force for any particle is given by:

$$F^{\text{Buoyancy}}_{\text{Particle}} = -\frac{4}{3}\pi\,(R_{\text{Particle}})^3 \Delta\rho_{\text{Particle}}\, g \quad (25)$$

where $\Delta\rho_{\text{Particle}} = \rho_{\text{Particle}} - \rho_{\text{Melt}}$, such that $F^{\text{Buoyancy}}_{\text{Particle}} > 0$ for positively buoyant particles and $F^{\text{Buoyancy}}_{\text{Particle}} < 0$ for negatively buoyant particles.

For a bubble–crystal pair, the net buoyancy force is given by:

$$F^{\text{Buoyancy}}_{\text{Net}} = F^{\text{Buoyancy}}_{\text{Mineral}} + F^{\text{Buoyancy}}_{\text{Bubble}} \quad (26)$$

The bubble–crystal pair is neutrally buoyant when the apparent weight of the crystal and the bubble are opposite and equal, such that $F^{\text{Buoyancy}}_{\text{Net}} = 0$. Assuming that both bubble and crystal are spherical, the ratio between the radii of mineral and bubble needed to obtain a neutrally buoyant pair can be computed:

$$F^{\text{Buoyancy}}_{\text{Net}} = \frac{4}{3}\pi\left[(R_{\text{Mineral}})^3 \Delta\rho_{\text{Mineral}} + (R_{\text{Bubble}})^3 \Delta\rho_{\text{Bubble}}\right] g = 0 \quad (27)$$

$$\frac{R_{\text{Mineral}}}{R_{\text{Bubble}}} = -\left(\frac{\Delta\rho_{\text{Bubble}}}{\Delta\rho_{\text{Mineral}}}\right)^{1/3} \quad (28)$$

Evidently, crystals are usually not spherical, such that R_{Mineral} is in fact the equivalent radius, i.e. the radius of the sphere with the same volume as the crystal, and can be used as a first order estimate of the size of the crystal.

Critical size of bubble–mineral pairs

In order to keep the neutrally buoyant bubble–mineral pair joined, the attachment force has to be equal to or larger than the separating force due to the difference in buoyancy of bubble and crystal. This separating force can be defined as:

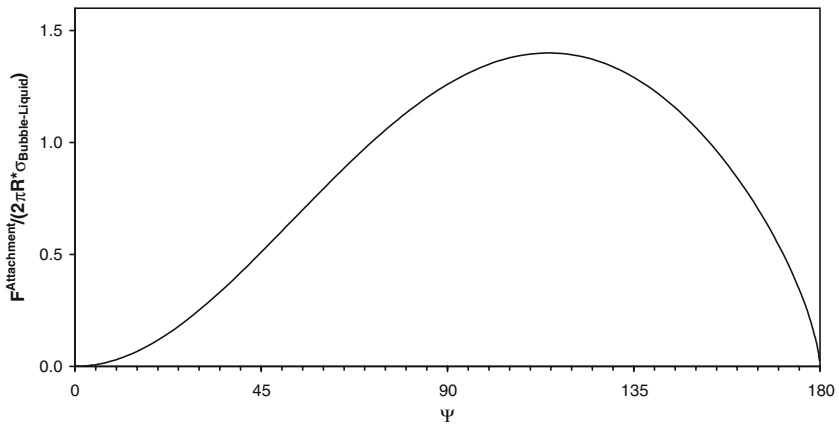

Fig. 4 Variation in the attachment force (normalized to a bubble perimeter 2πR and the bubble–liquid surface energy) as a function of the wetting angle Ψ. Note that $F^{\text{Attachment}}$ goes through a maximum at Ψ= 114.5°, which results from the attachment force depending not only on the vertical component of $\sigma_{\text{Bubble - Liquid}}$, but also on the radius of the contact surface, both of which are functions of the wetting angle

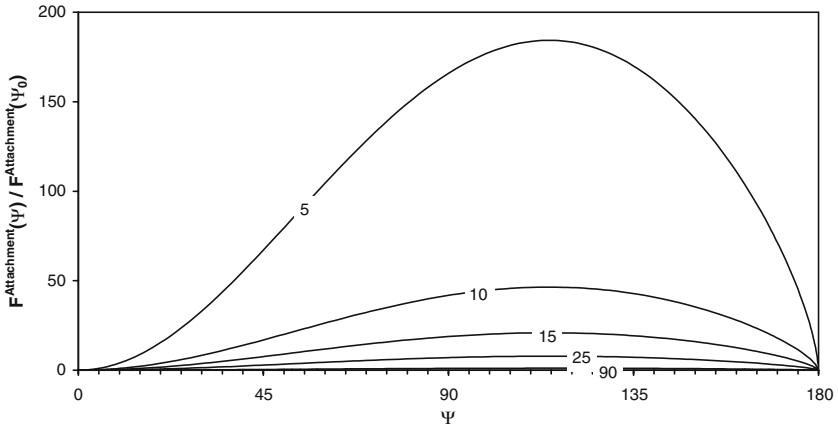

Fig. 5 Variation in the ratio between attachment force for two solids with wetting angles Ψ and Ψ_0 as a function of the wetting angle Ψ. Different curves correspond to distinct values of Ψ_0, as indicated. Variations in the ratio are relatively small for values of Ψ_0 larger than 15°

$$F^{\text{Buoyancy}}_{\text{Difference}} = F^{\text{Buoyancy}}_{\text{Mineral}} - F^{\text{Buoyancy}}_{\text{Bubble}} \tag{29}$$

When the bubble–crystal pair is neutrally buoyant, $F^{\text{Buoyancy}}_{\text{Mineral}}$ and $F^{\text{Buoyancy}}_{\text{Bubble}}$ are equal in magnitude but have opposite signs, such that Eq. 29 simplifies to:

$$F^{\text{Buoyancy}}_{\text{Difference}} = \frac{8}{3}\pi\,(R_{\text{Bubble}})^3 \Delta\rho_{\text{Bubble}}\, g \tag{30}$$

Since the attachment force is linear on R (Eq. 24), and the separating force is proportional to R cubed (Eq. 30), there is a limiting condition where $F^{\text{Buoyancy}}_{\text{Difference}} = F^{\text{Attachment}}$. From this condition, a bubble size can be determined, here called the critical bubble radius:

$$R^{\text{Critical}}_{\text{Bubble}} = \sqrt{-\frac{3\,\sigma_{\text{Bubble-Liquid}}}{4\,g\,\Delta\rho_{\text{Bubble}}}}\sin\theta \left[\frac{4}{2-3\cos(\theta)+\cos^3(\theta)}\right]^{1/6} \tag{31}$$

Neutrally buoyant pairs with a bubble of radius smaller than $R^{\text{Critical}}_{\text{Bubble}}$ will tend to remain attached, while, in the case of $R_{\text{Bubble}} > R^{\text{Critical}}_{\text{Bubble}}$, the attachment force will not be strong enough to keep the pair together. In all cases, the condition for neutral buoyancy is given by Eq. 28, such that the radius of the mineral is determined for a given bubble radius.

For bubbles smaller than the critical size, crystals with radii larger than that given by the buoyancy condition Eq. 28 can remain attached to the bubble, as long as the condition $F^{\text{Buoyancy}}_{\text{Difference}} \leq F^{\text{Attachment}}$ is satisfied, in which case the bubble–mineral pair would be negatively buoyant. Evidently, the presence of multiple crystals in a single bubble would also be possible, such that bubbles larger than the critical size could become neutrally or negatively buoyant. Naturally, given that the attachment of crystals to bubbles is always favored energetically (Eq. 18), formation of positively buoyant bubble–crystal pairs is always possible.

Application to natural magmas

We can now consider the formation of magnetite-bubble pairs in silicic melts. In particular, we are interested in the application of the formulation above to the early erupted Bishop Tuff.

For a rhyolitic magma of composition representative of the early erupted Bishop Tuff, appropriate values for the densities of the solid, melt and gas phases can be computed (Anderson and Liu unpublished data) as $\rho_{\text{Magnetite}} = 5.2$, $\rho_{\text{Quartz}} = 2.65$, $\rho_{\text{Melt}} = 2.15$, $\rho_{\text{Bubble}} = 0.4$ g/cm^3. The resulting radii ratios derived from Eq. 27 for magnetite and quartz are $R_{\text{Magnetite}}/R_{\text{Bubble}} = 0.83$ and $R_{\text{Quartz}}/R_{\text{Bubble}} = 1.52$.

In order to solve Eq. 31, absolute values of $\sigma_{\text{Bubble–Liquid}}$ must be known, ideally in conjunction with Ψ values for the same system. Such data are not available, and we use available values for $\sigma_{\text{Bubble–Liquid}}$ (Mangan and Sisson 2005) in conjunction with the Ψ values reported above (i.e. $\Psi_{\text{Magnetite}} = 35$, $\Psi_{\text{Quartz}} = 15$). Mangan and Sisson (2005) compile values for $\sigma_{\text{Bubble–Liquid}}$ obtained experimentally for systems of variable composition, from dacitic to rhyolitic, under variable water concentrations. In all cases, $\sigma_{\text{Bubble–Liquid}}$ is in the range 0.04–0.14 J/m^2, a rather narrow range given all simplifying assumptions and diversity of techniques used.

We can now calculate the critical bubble radii for magnetite and quartz in a rhyolitic melt (Table 1). The solution to the problem is illustrated graphically in Fig. 6, where F^{Buoyancy} and $F^{\text{Attachment}}$ are plotted for magnetite and quartz. Analysis of Fig. 6 and Table 1 shows that crystals larger than 1 mm in diameter could be attached to bubbles and form neutrally buoyant pairs.

Table 1 Values of the critical radii for bubble-magnetite and bubble-quartz pairs as a function of distinct values of bubble–liquid surface energy

	$\sigma_{\text{Bubble-Liquid}}$ (J/m^2)		
	0.04	0.09	0.14
Bubble critical radius (μm)	761	1,142	1,424
Magnetite critical radius (μm)	633	949	1,184
Bubble critical radius (μm)	342	513	640
Quartz critical radius (μm)	520	779	972

Gravitational force and Bond number

In Sect. 2.1 and 2.2, the theoretical treatment as presented ignored changes in bubble shape as well as changes in the wetting angle due to gravitational forces. Inclusion of gravitational effects makes the treatment much more complex (Adamson and Gast 1997), and is dealt with in specific literature on floatation (Boucher and Jones 1981; Rapacchietta and Neumann 1977; Rapacchietta et al. 1977; Smith and van de Ven 1985).

Smith and van de Ven (1985) present numerical solutions to the problem of a pendant fluid drop attached to a stationary spherical crystal, immersed in a second fluid. The solutions are such that they are valid for the case where the attached fluid is less dense that the surrounding liquid, analogous to the situation of interest here, where a crystal is attached to a bubble, and both immersed in a liquid. The details of the theoretical work by Smith and van de Ven (1985) are beyond the scope of this work. Importantly, however, they argue that the relevant dimensionless number for this problem is the Bond number, given by:

$$\text{Bond } \# = \frac{R^2_{\text{Mineral}}\,\Delta\rho_{\text{Bubble}}\,g}{\sigma_{\text{Bubble}-\text{Liquid}}} \tag{32}$$

The Bond number is the ratio between the gravitational forces and surface forces. Surface forces act to make the bubble spherical, while gravitational forces tend to distort the bubble from the spherical shape.

Figure 7 shows the variation of the Bond number with particle size for $\sigma_{\text{Bubble–Liquid}}$ in the range 0.04–0.14 J/m^2, and $\Delta\rho_{\text{Bubble}}$ = 1.75 g/cm^3. As expected, the importance of gravitational forces grows rapidly with increasing particle size. Table 1 shows that crystal critical radii are in the range 500–1,000 μm. For particles 1,000 μm in radius, the Bond number is between 0.12 and 0.43 (depending on σ), while for particles 500 μm in radius, the Bond number is in the range 0.03–0.11. In effect, the deformation of the

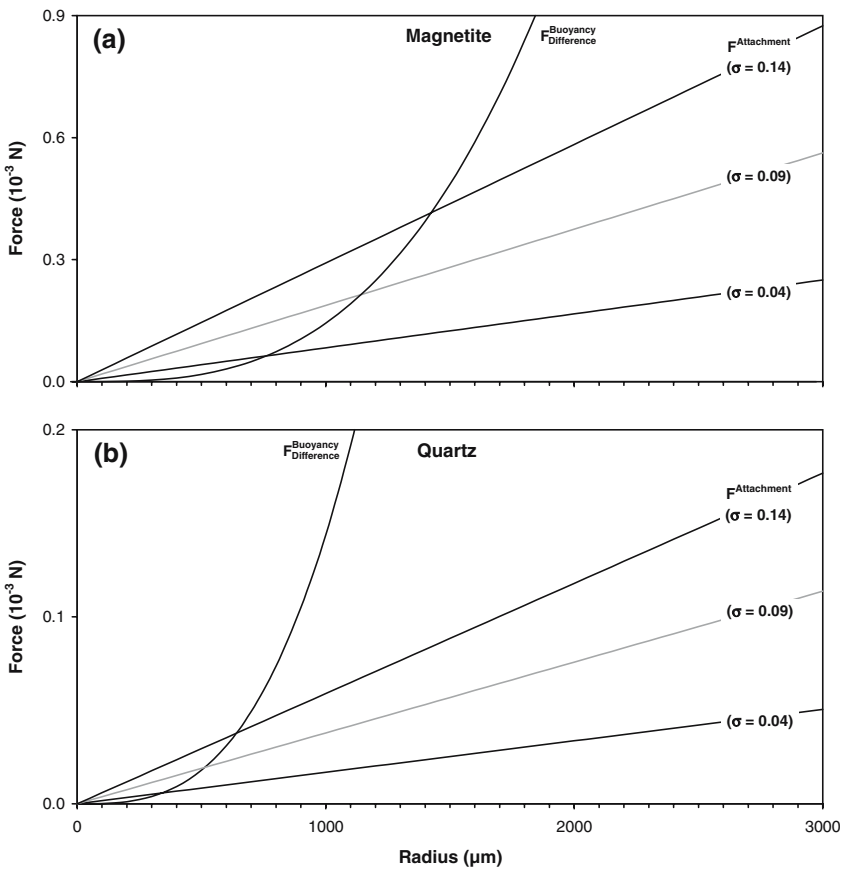

Fig. 6 Variations in the buoyancy and attachment forces as a function of the radius of the solid phase. Various curves for the attachment force correspond to distinct values for the bubble–liquid surface energy, as indicated. The point where $F^{\text{Buoyancy}} = F^{\text{Attachment}}$ corresponds to the critical radius for the solid phase (for bubble and melt with densities of 0.4 and 2.15 g/cm^3, respectively). The critical radius is defined here as the maximum size of a solid that can form a neutrally buoyant pair with a bubble and be held together by surface forces. Diagram **a** is for magnetite and **b** is for quartz. Diagram for sanidine (not shown) is almost identical to that for quartz given the similarity in density between the two minerals

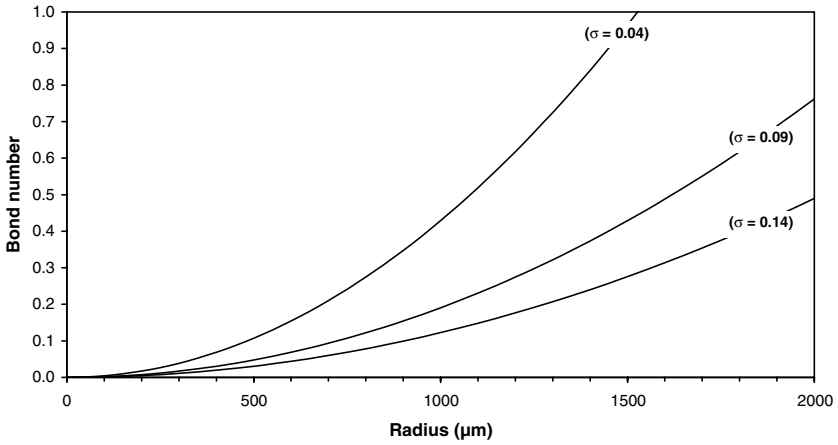

Fig. 7 Variation in the Bond number as a function of the radius of the solid particle. Various curves for the attachment force correspond to distinct values for the bubble–liquid surface energy, as indicated. For $R < 500$ μm, Bond number < 0.1, such that effect of gravity forces is negligible, such that the treatment presented here should be valid at least for particles 1 mm in diameter or smaller

bubble due to gravitational forces is negligible for particles <500 μm in radius, such that the treatment presented above should be applicable for particles as large as 1 mm in diameter.

Petrologic implications

From the theoretical considerations above, it can be concluded that: (1) attachment of magnetite crystals to bubbles is strongly favored over attachment of silicate minerals; (2) attachment of crystals to bubbles can lead to neutrally buoyant crystal–bubble aggregates; (3) magnetite crystals of at least several hundred μm (and maybe up to 1 mm) diameter can be held attached to a bubble of similar size by surface forces. Below, we explore some of the consequences of these to the evolution of silicic magmas, in particular the Bishop Tuff, for which a wealth of data is available.

A gas storage mechanism in pre-eruptive magmas

The possibility that bubbles may become neutrally buoyant by attaching magnetite crystals to them gives rise to the idea that magmas may be characterized by a permanent bubble population that is dynamically stagnant relative to the melt. We are particularly interested in testing whether this mechanism can account for the bubble abundance inferred to exist in the pre-eruptive Bishop magma (Wallace et al. 1995, 1999).

Based on the evolution of H_2O/CO_2 ratios in melt inclusions, Wallace et al. (1995) argued that an exsolved gas phase had to be present during differentiation and crystallization of the Bishop rhyolitic magma. They estimated the amount of exsolved gas present to be 3–6 wt% (14–25 vol%) in the early, 1–3 wt% in the middle, and ~0.5 wt% in the late-erupted Bishop magma.

We have recently studied in detail the textures of three pumice clasts from the early erupted Bishop Tuff (Gualda 2006; Gualda et al. 2004; Gualda and Rivers 2006). Relative abundances, as well as crystal size distributions, are available for quartz, sanidine and magnetite crystals in these samples, and can be used to infer the maximum proportion of gas that can be stored as neutrally buoyant bubble–crystal aggregates.

As argued above, magnetite is much more likely to be attached to bubble surfaces than other crystals. Under the limiting assumption that all magnetite crystals form neutrally buoyant pairs with gas bubbles, from Eq. 28, it is possible to compute the maximum gas volume fraction that can be stored as neutrally buoyant bubble–magnetite aggregates. In the samples studied by Gualda and Rivers (2006), magnetite corresponds to about 1% of the total crystal volume. The crystal volume fraction (i.e. crystal volume/[crystal volume + glass volume]) is close to 10%, such that the total abundance of magnetite is only ca. 0.1 vol%. This yields maximum gas volume fractions on the order of 0.1–0.2 vol%. These values are at least one order of magnitude lower than the values calculated by Wallace et al. (1995). An even more extreme assumption can be made, by considering that all crystals (i.e. not only magnetite) are associated to bubbles and form neutrally buoyant bubble–crystal aggregates. In this extreme case, 2–3 vol% of gas could be accounted for.

It becomes clear that the formation of neutrally buoyant crystal–bubble aggregates cannot explain the abundance of exsolved gas inferred by Wallace et al. (1995) for the early erupted Bishop magma. Nonetheless, the recognition of a large vesicle with abundant magnetite crystals attached to its walls forming a nearly neutrally buoyant aggregate (Gualda and Anderson 2007) suggests that this is indeed a viable mechanism for storing exsolved gas in magmas. In the case of the early erupted Bishop magma, the inevitable conclusion seems to be that a range of pre-eruptive bubbles

existed, from magnetite-free, to magnetite-rich bubbles. The figures above suggest that only a very small fraction of the pre-eruptive bubbles—possibly on the order of 1–2%—may be attached to magnetite crystals. In this sense, the recognition of a bubble–magnetite aggregate (Gualda and Anderson 2007) is quite fortunate, given the small sample volumes analyzed so far.

Magnetite-bubble association: not so simple!

One of the main conclusions from the above discussion is that there should be an intrinsic association between magnetite crystals and bubbles. That such an association is present is clearly shown by decompression experiments (Hurwitz and Navon 1994; Mangan and Sisson 2000, 2005) and by some petrographic observations (Gualda and Anderson 2007). However, study of our tomography datasets shows that most magnetite crystals are free of bubbles (Fig. 8; Video 1). Not only is this surprising, but also relevant to the understanding of nucleation under pre-eruptive conditions.

In particular, there is abundant experimental evidence that magnetite crystals are the predominant nucleation sites for bubbles at low degrees of supersaturation. At higher degrees of supersaturation, the barrier for homogeneous nucleation can be superseded, such that nucleation does not take place exclusively on magnetite crystals (Hurwitz and Navon 1994; Mangan and Sisson 2000, 2005). There is no apparent reason to believe, however, that heterogeneous nucleation should cease at this stage, given that the energy barrier for heterogeneous nucleation is always smaller than that for homogeneous nucleation (Adamson and Gast 1997). In this context, it is quite remarkable that magnetite crystals in the early erupted Bishop Tuff do not commonly have vesicles associated to them. The puzzling conclusion that arises from this observation is that somehow, nucleation away from crystals (homogeneous nucleation?) is favored over heterogeneous nucleation on crystal substrates. Solids with even larger wetting angles could be present in the melt as impurities, and could be strongly favored over magnetite as nucleation sites; while it is conceivable that such impurities would be of difficult detection due to their minute size, there is no evidence to support this hypothesis. Another aspect not taken in consideration is the strain state of the melt, which could favor ''homogeneous'' over heterogeneous nucleation (Anderson 2006). These two possibilities are rather speculative, however, and future research should be aimed at addressing this problem.

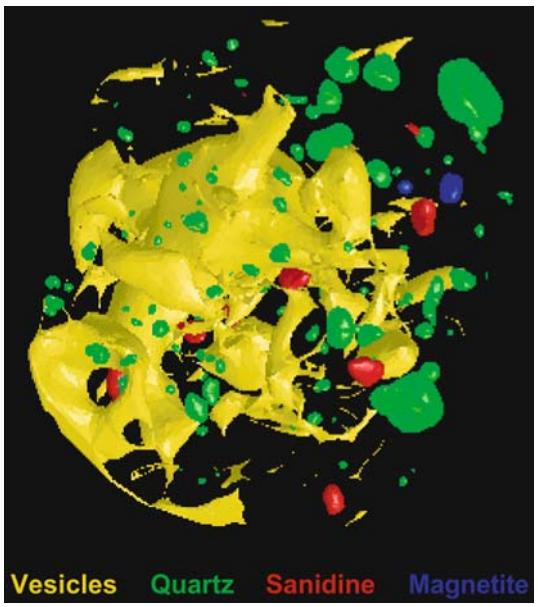

Fig. 8 Three-dimensional view of Sample F7–12; glass was suppressed for clarity. Magnetite crystals are *shaded dark gray* (*blue* in the online version), feldspar intermediate *gray* (*red*), quartz *light gray* (*green*), and vesicles *very light gray* (*yellow*). Notice that most crystals are not attached to large vesicles. Small vesicles (<50 μm) are suppressed from this view. Field of view is ca. 8 × 7 mm. An animated version of this figure is available online as Video 1

Conclusions

In this contribution, we review the fundamentals of the energetics of bubble–crystal surface interactions and derive equations that can explain the usual association between bubbles and magnetite crystals indicated by experiments and some isolated observations.

We define the attachment energy as the surface energy change due to attachment of a crystal to a bubble. We show that attaching a bubble to a mineral substrate is always energetically favored over keeping bubble and mineral separate. Because the attachment energy is a strong function of the wetting angle, different minerals will be more strongly attached to bubbles than others. In particular, oxide minerals will attach to a given bubble much more strongly than any silicates in silicate melts. The barriers to attachment and detachment increase with increasing wetting angle, such that the efficiency of attachment should decrease with increasing wetting angle (i.e. from silicates to oxides); at the same time, once attached, it becomes more difficult to detach bubble from crystal for large wetting angles.

One interesting consequence of the attachment of grains to a bubble is that this can cause these bubble–crystal pairs to be neutrally buoyant, preventing bubble rise and crystal sinking. From the definition of the wetting angle, we derive an expression for the attachment force, and show that neutrally buoyant aggregates consisting of crystals up to

1 mm diameter and bubbles of similar size can be held attached by surface forces.

While gravitational forces will deform the bubble and change the wetting angle, for particles smaller than 1 mm, the contribution of gravitational forces is negligible, such that the treatment presented here should be valid.

Under the limiting assumption that all magnetite crystals form neutrally buoyant pairs with bubbles, the maximum gas volume fraction that can be stored as neutrally buoyant bubble–magnetite aggregates is orders of magnitude smaller than the abundance of exsolved gas inferred from melt inclusions in the Bishop magma (Wallace et al. 1995). Nonetheless, our recent observation of one such aggregate in the early erupted Bishop Tuff (Gualda and Anderson 2007) suggests that this is indeed a viable mechanism for storing exsolved gas in magmas, such that a range of pre-eruptive bubbles existed, from magnetite-free, to magnetite-rich bubbles. Yet, only a very small fraction of them could have magnetite crystals attached to them.

Our treatment shows that there should be an intrinsic association between magnetite crystals and bubbles. However, the existing evidence for Bishop pumice clasts reveals bubble-free magnetite crystals, which leads to the puzzling conclusion that ''homogeneous'' nucleation is favored over heterogeneous nucleation on crystal substrates.

Acknowledgments We have benefited greatly from stimulating discussions with Alfred Anderson and Bruce Buffett. We would also like to acknowledge NSF support (EAR-0408707) to A. T. Anderson.

References

Adamson AW, Gast AP (1997) Physical chemistry of surfaces. Wiley, New York, p 784

Anderson AT (2006) Bubbleless glass pockets and natural bubble nucleation in rhyolitic magma. Eos Trans AGU 87(52): Fall Meet Supplement, Abstract V43A–1785

Boucher EA, Jones TGJ (1981) Empirical criteria for the flotation of a solid sphere at an interface in a gravitational-field. J Colloid Interface Sci 83(2):645–648

Gualda GAR (2006) Crystal size distributions derived from 3D datasets: sample size versus uncertainties. J Petrol 47(6):1245–1254

Gualda GAR, Anderson AT (2007) Magnetite scavenging and the buoyancy of bubbles in magmas. Part 1: Discovery of a pre-eruptive bubble in Bishop rhyolite. Contrib Mineral Petrol 153(6):733–742

Gualda GAR, Rivers M (2006) Quantitative 3D petrography using X-ray tomography: application to bishop tuff pumice clasts. J Volcanol Geoth Res 154(1–2):48–62

Gualda GAR, Cook DL, Chopra R, Qin LP, Anderson AT, Rivers M (2004) Fragmentation, nucleation and migration of crystals and bubbles in the Bishop Tuff rhyolitic magma. T R Soc Edin Earth 95:375–390

Hurwitz S, Navon O (1994) Bubble nucleation in rhyolitic melts—experiments at high-pressure, temperature, and water-content. Earth Planet Sci Lett 122(3–4):267–280

Laporte D (1994) Wetting behavior of partial melts during crustal anatexis—the distribution of hydrous silicic melts in polycrystalline aggregates of quartz. Contrib Mineral Petrol 116(4):486–499

Mangan M, Sisson T (2000) Delayed, disequilibrium degassing in rhyolite magma: decompression experiments and implications for explosive volcanism. Earth Planet Sci Lett 183(3–4):441–455

Mangan M, Sisson T (2005) Evolution of melt-vapor surface tension in silicic volcanic systems: experiments with hydrous melts. J Geophys Res Sol Ea 110(B1)

Mangan MT, Sisson TW, Hankins WB (2004) Decompression experiments identify kinetic controls on explosive silicic eruptions. Geophys Res Lett 31(8)

Mysen BO, Richet P (2005) Silicate glasses and melts: properties and structure. Elsevier, Amsterdam, p 544

Rapacchietta AV, Neumann AW (1977) Force and free-energy analyses of small particles at fluid interfaces. 2. Spheres. J Colloid Interface Sci 59(3):555–567

Rapacchietta AV, Neumann AW, Omenyi SN (1977) Force and free-energy analyses of small particles at fluid interfaces. 1. Cylinders. J Colloid Interface Sci 59(3):541–554

Schafer FN, Foley SF (2002) The effect of crystal orientation on the wetting behaviour of silicate melts on the surfaces of spinel peridotite minerals. Contrib Mineral Petrol 143(2):254–261

Smith PG, van de Ven TGM (1985) The separation of a liquid–drop from a stationary solid sphere in a gravitational-field. J Colloid Interface Sci 105(1):7–20

Wallace PJ, Anderson AT, Davis AM (1995) Quantification of pre-eruptive exsolved gas contents in silicic magmas. Nature 377(6550):612–616

Wallace PJ, Anderson AT, Davis AM (1999) Gradients in H_2O, CO_2, and exsolved gas in a large-volume silicic magma system: Interpreting the record preserved in melt inclusions from the Bishop Tuff. J Geophys Res Sol Ea 104(B9):20097–20122

Weisstein EW (2007) Spherical Cap. From MathWorld–A Wolfram Web Resource. http://www.mathworld.wolfram.com/SphericalCap.html

Wilson L, Sparks RSJ, Walker GPL (1980) Explosive volcanic-eruptions. 4. The control of magma properties and conduit geometry on eruption column behavior. Geophys J R Astron Soc 63(1):117–148